J Solid State Electrochem (2008) 12:591–599
DOI 10.1007/s10008-007-0416-z

ORIGINAL PAPER

Effect of thermal treatment on phase composition and ethanol oxidation activity of a carbon supported Pt50Sn50 alloy catalyst

F. Colmati · E. Antolini · E. R. Gonzalez

Published online: 14 September 2007

Abstract A carbon supported Pt–Sn electrocatalyst in the Pt/Sn atomic ratio 50:50 was prepared by the reduction of Pt and Sn precursors with formic acid and thermally treated at 200 °C (i.e., in the presence of solid tin) and 500 °C (in the presence of molten tin) in flowing hydrogen. In the absence of thermal treatment, X-ray diffraction (XRD) analysis showed a solid solution of Sn in the face centered cubic (fcc) Pt and SnO_2. After thermal treatment, the formation of a main phase of hexagonal PtSn (niggliite) and a secondary phase of cubic Pt_3Sn was observed in the Pt50Sn50 catalyst. The relative amount of the PtSn phase increased with increasing thermal treatment temperature. The presence of molten tin gave rise to the formation of some big particles during annealing at 500 °C. The activity for the ethanol oxidation reaction (EOR) of the as-prepared catalyst was higher than that of both thermally treated catalysts and Pt75Sn25/C and Pt50Ru50/C by E-TEK. The higher activity for the EOR of the as-prepared Pt–Sn catalysts was ascribed to the presence of a large amount of SnO_2.

Keywords Pt–Sn alloys · Supported catalysts · Ethanol oxidation · Electrocatalysis

Introduction

Within the efforts to identify fuels for fuel cells, ethanol is considered to be attractive because of its non-toxicity, renewability, high power density, and low green-house effect in the atmosphere when produced from biomass. Pure Pt is not the most efficient anodic catalyst for the direct ethanol fuel cell because it is known to be rapidly poisoned by strongly adsorbed species coming from the dissociative adsorption of ethanol [1]. Indeed, the electrooxidation of a partially oxygenated organic molecule, such as a primary alcohol, can only be performed with a multifunctional electrocatalyst. Preliminary works [2, 3] indicated that the modification of Pt by tin gives very interesting results leading to the oxidation of ethanol at lower potentials than on pure platinum. Therefore, to understand better the effect of tin on the electrocatalytic activity of platinum, it becomes important to know the characteristics of Pt–Sn bimetallic alloys. Platinum and tin form five bimetallic intermetallic phases, Pt_3Sn, PtSn, Pt_2Sn_3, $PtSn_2$, and $PtSn_4$, of which Pt_3Sn and PtSn are congruently melting compositions. The PtSn phase is commonly known as the mineral niggliite. These intermetallic phases are distinguished by distinct crystalline structures and unique X-ray diffraction (XRD) patterns.

Bimetallic nanoparticles supported on a high surface area conducting substrate find widespread application as electrode materials. Many studies have been carried out in the past decades on silica and alumina supported Pt–Sn with low platinum loadings (<5 wt%) [4–9] and on carbon supported Pt–Sn catalysts with high platinum loading (>5 wt%) [1, 10–14]. Some of these catalysts were tested as anode materials for direct ethanol fuel cells (DEFCs). Zhou et al. [12] prepared by modified polyol method and tested in DEFCs carbon supported Pt–Sn alloy particles with nominal Pt/Sn ratios in the range 4:1 to 1:1 and a Pt loading of 20 wt%. They found that the Pt–Sn catalysts had a prevailing Pt (face centered cubic, fcc) crystal structure with the XRD reflexions shifted to lower angles, which means that part of the Sn present in the catalyst is alloyed

Dedicated to Teresa Iwasita's 65th birthday.

F. Colmati · E. Antolini · E. R. Gonzalez (✉)
Instituto de Química de São Carlos, USP,
CP 780,
São Carlos, SP 13560-970, Brazil
e-mail: ernesto@iqsc.usp.br

with Pt. The lattice parameter of crystalline Pt increased as the Sn content increased. All Pt–Sn catalysts had very similar particle sizes ranging between 2.2 and 3.0 nm. Single direct ethanol fuel cells having either Pt–Sn/C (1:1) or Pt–Sn/C (3:2) or Pt–Sn/C (2:1) as anode catalyst showed better performances than those with Pt–Sn/C (3:1), Pt–Sn/C (4:1), or Pt/C. Lamy et al. [1] prepared from colloidal precursors Pt–Sn particles dispersed on carbon powder (Vulcan XC72) (Pt/Sn atomic ratio from 9:1 to 1:1, metal loading 30 and 60 wt%), using the well-known "Bönnemann" method [13]. In the case of Pt–Sn (9:1), the absence of shifts in the Pt diffraction peaks showed that no alloy is formed during the co-reduction process. For higher Sn contents, a small shift of the Pt diffraction peaks was observed, suggesting a partial alloying of Pt–Sn particles, probably forming cubic Pt_3Sn clusters. The mean particle diameter was 2.6±1.3 nm. No significant particle size change was observed when the Pt–Sn atomic composition changed from 1:1 to 9:1. The results of half-cell and direct ethanol fuel cell tests indicate that the overall electrocatalytic activity of Pt is greatly enhanced at low potentials by the presence of tin. The optimum composition was in the range 10–20 at. Sn%.

In our previous work [14], we prepared, by the formic acid method (FAM), carbon supported Pt–Sn catalysts with nominal Pt/Sn ratios 9:1, 3:1, and 2:1 and metal loading 20 wt%. The lattice parameter of the Pt fcc structure, the particle size by transmission electron microscopy (TEM), and the DEFC performance increased with the Sn content in the catalyst.

In this work, a carbon-supported Pt–Sn catalysts in the Pt/Sn atomic ratio 1:1 and metal loading 20 wt% was prepared using FAM, and the effect of the thermal treatment on the structural characteristic of the Pt50Sn50/C catalyst was investigated. The activities for ethanol oxidation of the as-prepared and thermally treated Pt50Sn50/C catalysts were studied by linear sweep voltammetry (LSV) and chroamperometry (CA) and compared with those of commercial Pt75Sn25/C and Pt50Ru50/C catalysts. Taking into account that the melting temperature of tin is 231.9 °C, thermal treatments were carried out at 200 °C (in the presence of solid tin) and 500 °C (in the presence of molten tin).

Experimental

Catalyst preparation

The Pt50Sn50/C electrocatalyst was prepared by the FAM [15]. An appropriated mass of the carbon powder substrate (Vulcan XC-72, Cabot, 240 $m^2\ g^{-1}$) is suspended in 2 mol l^{-1} formic acid solution, and the suspension is heated to 80 °C. Chloroplatinic acid ($H_2PtCl_6.6H_2O$, Johnson Matthey) solution and a tin chloride ($SnCl_2.2H_2O$, Merck) solution were slowly added to the carbon suspension. The suspension was left to cool at room temperature and the solid filtered and dried in an oven at 80 °C for 1 h. The materials were 20% (*w*/*w*) metal (Pt + Sn) on carbon. Portions of the as-prepared catalyst were thermally treated at 200 and 500 °C for 1 h under flowing H_2.

Energy dispersive X-ray analysis

The atomic ratios of the Pt–Sn/C catalyst were determined by the energy dispersive X-ray analysis (EDX) technique coupled to a scanning electron microscope LEO Mod. 440 with a silicon detector with Be window and applying 20 keV.

X-ray diffraction

X-ray diffractograms of the catalysts were obtained at the D12A-XRD1 beam line of the Brazilian Synchrotron Light Laboratory. Scans were done for 2θ values between 20 and 100°. The lattice parameters were obtained by refining the unit cell dimensions by the least squares method.

High resolution transmission electron microscopy

The samples for the high resolution transmission electron microscopy (HRTEM) characterizations were prepared as follows: a carbon film was deposited onto a mica sheet that was placed onto the Cu grids (300 mesh and 3 mm diameter). The material to be examined was dispersed in water by sonication, placed onto the carbon film, and left to dry. Histograms of particle sizes were constructed using about 300 particles.

This technique was implemented in the Microscopy Laboratory of the Brazilian Synchrotron Light Laboratory using a HRTEM microscope JEOL, JEM 3010, URP, operating at 300 kV and having a resolution of 0.17 nm.

Electrochemical measurements

To test the activity for the oxidation of ethanol, the electrocatalysts were used to make two-layer gas diffusion electrodes. A diffusion layer was made with carbon powder (Vulcan XC-72R) and 15 wt% (*w*/*w*) polytetrafluoroethylene (PTFE) and applied over a carbon cloth (PWB-3, Stackpole). On top of this layer, the electrocatalyst was applied in the form of a homogeneous dispersion with Nafion® solution (5 wt%, Aldrich) and isopropanol (Merck). All electrodes were made to contain 1 mg Pt cm^{-2}. For the direct ethanol single-cell studies, the electrodes were hot pressed on both sides of a Nafion® 115 membrane at 125 °C and 50 kg cm^{-2} for 2 min. The geometric area of the electrodes was 4.6 cm^2, and the cathode material was 20 wt% Pt/C from E-TEK.

LSV curves were recorded at room temperature, 40 and 90 °C in the range 0.1–0.8 V vs a reversible hydrogen electrode (RHE). Cyclic voltammetry (CV) curves were recorded in the range 0.1–1.0 V vs RHE. The sweep rate was 20 mV s^{-1}. Chronoamperometry measurements were performed at 90 °C at 0.5 V for 3,600 s. The oxidation of ethanol on Pt50Sn50/C prepared by the FAM and Pt75Sn25/C and Pt50Ru50/C from E-TEK catalysts was tested in a direct ethanol fuel cell system fed with a 1.0 M ethanol solution at the anode. Hydrogen was supplied to the cathode, which operated simultaneously as auxiliary and reference electrode. The experiments were done at room temperature, 40 and 90 °C with a 1285 A Solartron Potentiostat connected to a personal computer and using the software CorrWare for Windows (Scribner).

Results

Elemental analysis from different regions of the carbon supported Pt–Sn particles was conducted with EDX analysis. The mean Pt/Sn atomic ratio was 51:49, very close to the nominal value.

Figure 1a shows the whole XRD patterns of the as-prepared and thermally treated carbon-supported Pt–Sn alloy catalysts. As can be seen in Fig. 1a, the XRD pattern of the as-prepared catalyst shows the characteristic peaks of the fcc crystalline Pt. These diffraction peaks are slightly shifted to lower 2θ values in the Pt–Sn alloy catalysts with respect to the corresponding peaks in the pure Pt catalyst. No peaks for either cubic Pt_3Sn or hexagonal PtSn phases were detected. The lattice parameter obtained from the (311) peak of the as-prepared catalyst was 0.3973 nm, higher than that of pure Pt/C (a_o=0.39075 nm [16]) and lower than that of the Pt_3Sn/C phase (a_o=0.40015 nm [17]) with comparable particle sizes. Regarding the values of the Pt–Sn lattice parameter, Kuznetzov et al. [18] asserted that Pt forms nearly all possible alloys with Sn. Radmilovic et al. [10], instead, attributed the value of the lattice constant of 0.3965 nm, found for a commercial carbon supported Pt/Sn 1.23/1 catalyst, to a mixture of Pt_9Sn (0.3934 nm) [19] and Pt_3Sn phases. The presence of SnO_2 reflexions was observed in the XRD pattern of the as-prepared Pt–Sn catalysts, at 2θ angles of 33.76 and 51.58°, associated with the (101) and (211) planes of tetragonal SnO_2. Figure 1b shows detailed SnO_2 (211) peak.

The crystallite size of the Pt–Sn alloy nanoparticles was estimated using Scherrer's equation $d=0.94k_1/B_{(2)}\cos\theta$, where d is the average crystallite diameter, k_1 is the wavelength of X-ray radiation (0.154056 nm), θ is the position of the (311) diffraction peak, and $B_{(2)}$ is the width in radians of the diffraction peak at half height. The calculated average crystallite size of the as-prepared Pt–Sn/C catalyst was 3.6 nm

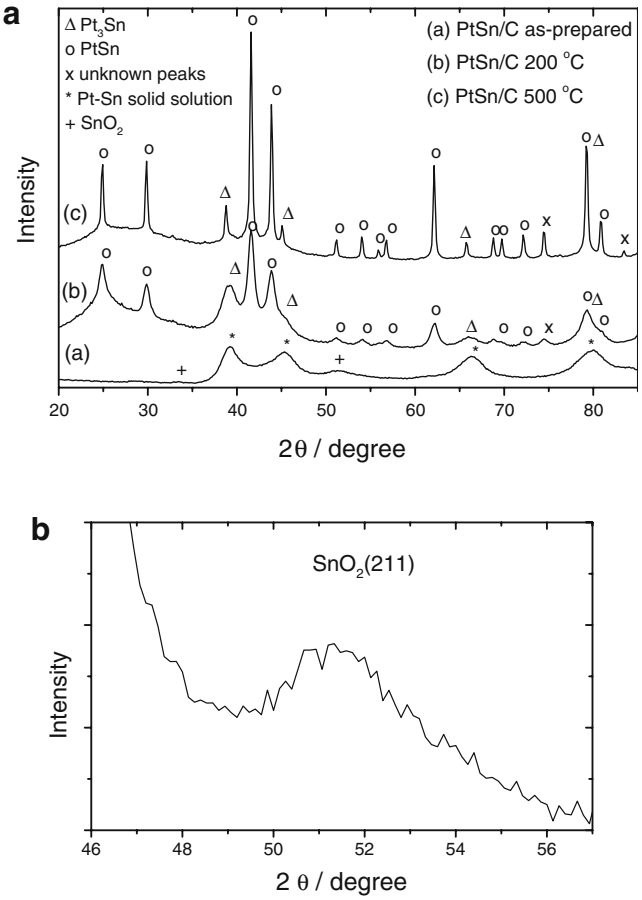

Fig. 1 XRD patterns of as-prepared and thermally treated at 200 and 500 °C Pt50Sn50/C catalyst. **a** Whole XRD patterns; **b** detail of the SnO_2 (211) peak

The reduction of $Sn^{4+}$and Sn^{2+}, eventually present, to Sn^0 took place with thermal treatment in a hydrogen atmosphere. As can be inferred from the XRD patterns, the formation of cubic fcc Pt_3Sn and hexagonal hcp PtSn phases took place after the thermal treatment at both temperatures. The reduced tin reacted with the fcc Pt-Sn solid solution to form Pt_3Sn and PtSn (niggliite) phases. The Pt_3Sn lattice parameters were calculated using the (220) reflexion, being the (311) overlapped with the PtSn (212) reflexion, and the results are reported in Table 1. After thermal treatment at 200 °C, the Pt_3Sn lattice constant showed the nearly stoichiometric value; a lattice parameter slightly higher than the stoichiometric value was obtained after thermal treatment at 500 °C, perhaps due to an Sn excess.

Regarding the PtSn phase, the positions of the PtSn (100), (110), (200), and (300) diffraction peaks were used to calculate the a_o lattice constants, and the positions of the PtSn (004) diffraction peaks were used to calculate the corresponding c_o lattice constants. The diffraction peaks of the PtSn phase were slightly shifted to lower 2θ values with respect to the corresponding peaks in the stoichiometric hexagonal PtSn catalyst. For both thermally treated

Table 1 Lattice parameters and crystallite size of Pt_3Sn and PtSn phases and $Pt_3Sn(111)/PtSn(102)$ peak intensity ratios in Pt50Sn50 thermally treated at 200 and 500 °C

Catalyst	fcc Pt3Sn		hcp PtSn		Peak intensity ratio
	Lattice constant (nm)	Crystallite size (nm)	Lattice constants (nm)	Crystallite size (nm)	Pt3Sn(111)/PtSn(102)
PtSn/C (50:50) 200 °C	a_o=0.3999	n.d.	a_o=0.4117 c_o=0.5452	10	0.40
PtSn/C (50:50) 500 °C	a_o=0.4013	30	a_o=0.4117 c_o=0.5452	29	0.17

samples, the calculated lattice constants were a_o=0.4117 nm and c_o=0.5453 nm, higher than those of the stoichiometric PtSn (a_o=0.4103 nm, c_o=0.5428 nm). However, the c/a ratio was the same as that of stoichiometric PtSn (c/a= 1.32), indicating that with the thermal treatment an expansion of the unit cell volume occurred, without preferential orientation. As the radius of the Sn atom is larger than that of the Pt atom, the substitution of Pt with Sn leads to an expanded unit cell volume. Therefore, the formation of a non-stoichiometric Sn-rich hcp PtSn phase is likely. The peak intensity ratios of the reflexions of Pt_3Sn and PtSn phases were calculated from the XRD patterns of thermally treated samples and reported in Table 1. The $Pt_3Sn(111)/PtSn(102)$ peak intensity ratio decreased with increasing thermal treatment temperature, i.e., the relative amount of the hexagonal phase increased with increasing annealing temperature.

Figures 2, 3, and 4 present the results of the HRTEM analysis of the as-prepared and thermally treated carbon-supported Pt50Sn50 catalysts prepared by the FAM. HRTEM micrographs were obtained with magnifications in the range 150,000–800,000. Low-magnification images (part A of the figures) show that, in the as-prepared and 200 °C thermally treated catalysts, the distribution of the metal particles on the carbon support is uniform and in a narrow particle size range. The histograms of the particle size distribution (part B of the figures), which include analyses of several different regions, reflect quantitatively the uniform distribution in these catalysts. Conversely, the image of the Pt–Sn catalyst thermally treated at 500 °C shows the presence of some big particles (>30 nm) together with particles having a smaller size and in a narrow particle size range. The mean particle diameter, d, was calculated with Eq. 1,

$$d = \Sigma(k) n_k d_k / n_k \quad (1)$$

where n_k is the frequency of occurrence of particles with size d_k. The particle size for the as-prepared Pt50Sn50/C catalyst was between 3 and 10 nm, with a mean diameter of 6.6 nm. This value is sensibly higher than the value of the crystallite size from XRD. A possible explanation for the discrepancy is the following: the XRD peak broadening is due not only to the crystallite size but also to non-homogeneity of the solid solution (as previously reported, the fcc Pt–Sn peaks in the as-prepared catalyst are probably formed by the overlapping of the Pt_9Sn and Pt_3Sn reflexions), then the crystallite size calculated by XRD is smaller than the particle size. The dependence of the average Pt–Sn particle size determined by TEM of the Pt–Sn/C catalysts prepared by the FAM on Sn content in the catalyst is shown in Fig. 5. The values of the particle sizes of the Pt–Sn/C catalysts with nominal ratio Pt/Sn>1 were obtained from [14]. Surprisingly, the size of the Pt–Sn particles increased with Sn content. Indeed, at constant metal loading the number of Pt atoms decreases with increasing Sn content, and as a consequence, the Pt–Sn particle size should decrease. This behavior could be explained by the competition between Pt atoms to nucleate fcc Pt–Sn particles and Sn atoms to nucleate SnO_2 particles considering the interaction with the active sites of the carbon support.

The particle size for the Pt50Sn50/C catalyst thermally treated at 200 °C was between 3.5 and 14.5 nm, with a mean diameter of 8.6 nm, which agrees with the value of the crystallite size of the PtSn phase calculated by XRD. The slight increase in particle size with respect to the as-prepared catalyst is due to the incorporation of Sn in the fcc Pt–Sn solid solution to form the Pt_3Sn and PtSn phases.

The particle size for the Pt50Sn50/C catalyst thermally treated at 500 °C was between 3 and 74.5 nm, with a mean diameter of 13.6 nm. The discrepancy between the average particle size from TEM and the crystallite size from XRD (approximately 30 nm for both the Pt_3Sn and the PtSn phases) can be ascribed to the prevailing effect of the large crystallites on the intensity of the XRD reflexions. Limiting the count to particles with size <20 nm, the histogram of the catalyst annealed at 500 °C presents a uniform distribution with an average particle size of 11.4 nm. Part C of Figs. 2, 3, and 4 show high-magnification HRTEM micrographs, which reveal the asymmetric faceted shape, typically cubooctahedral, of Pt–Sn particles. However, in some cases, the two-dimensional projection gives the impression of spherical or elliptical shapes. The presence of large

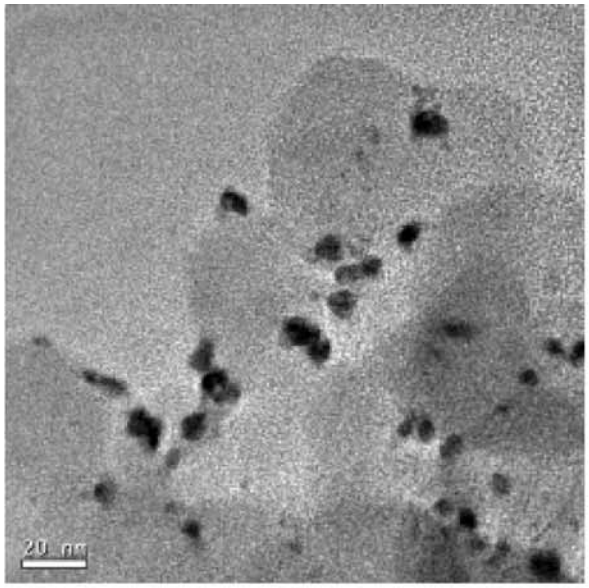

a

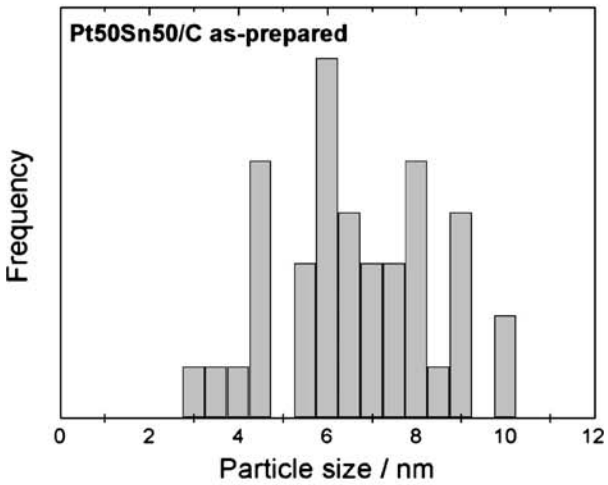

b

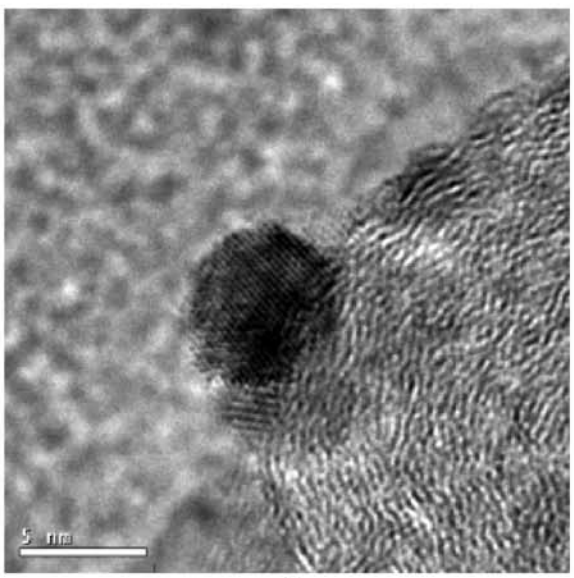

c

◀ **Fig. 2** **a** Low-magnification HRTEM micrograph. **b** Particle size distribution determined from the HRTEM micrographs. **c** High-magnification HRTEM micrograph of the as-prepared Pt50Sn50/C catalyst

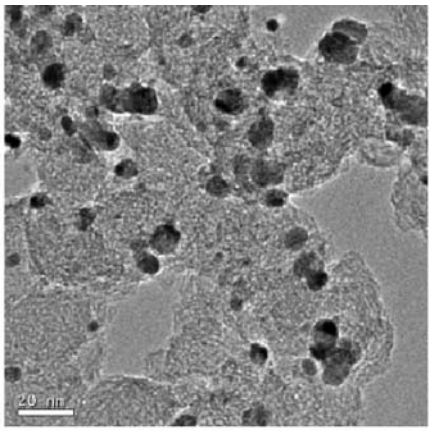

a

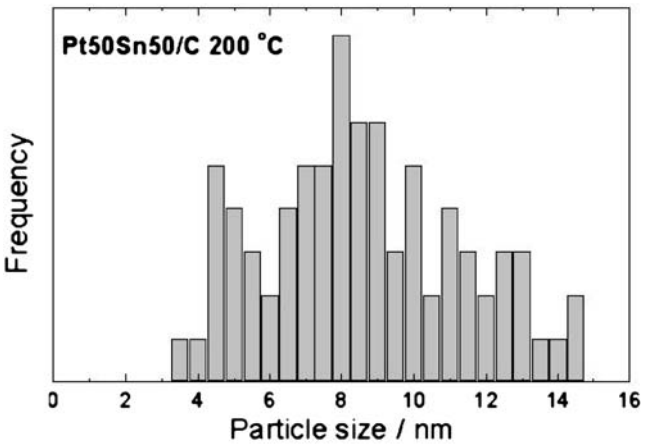

b

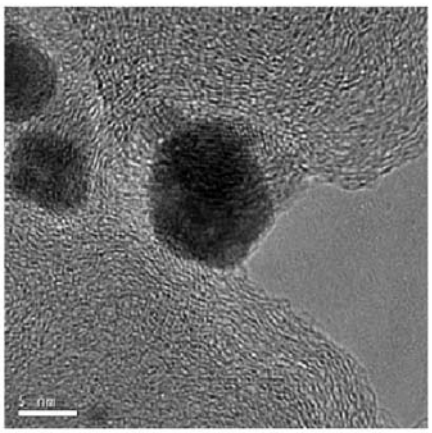

c

Fig. 3 **a** Low-magnification HRTEM micrograph. **b** Particle size distribution determined from the HRTEM micrographs. **c** High-magnification HRTEM micrograph of the Pt50Sn50/C catalyst thermally treated at 200 °C

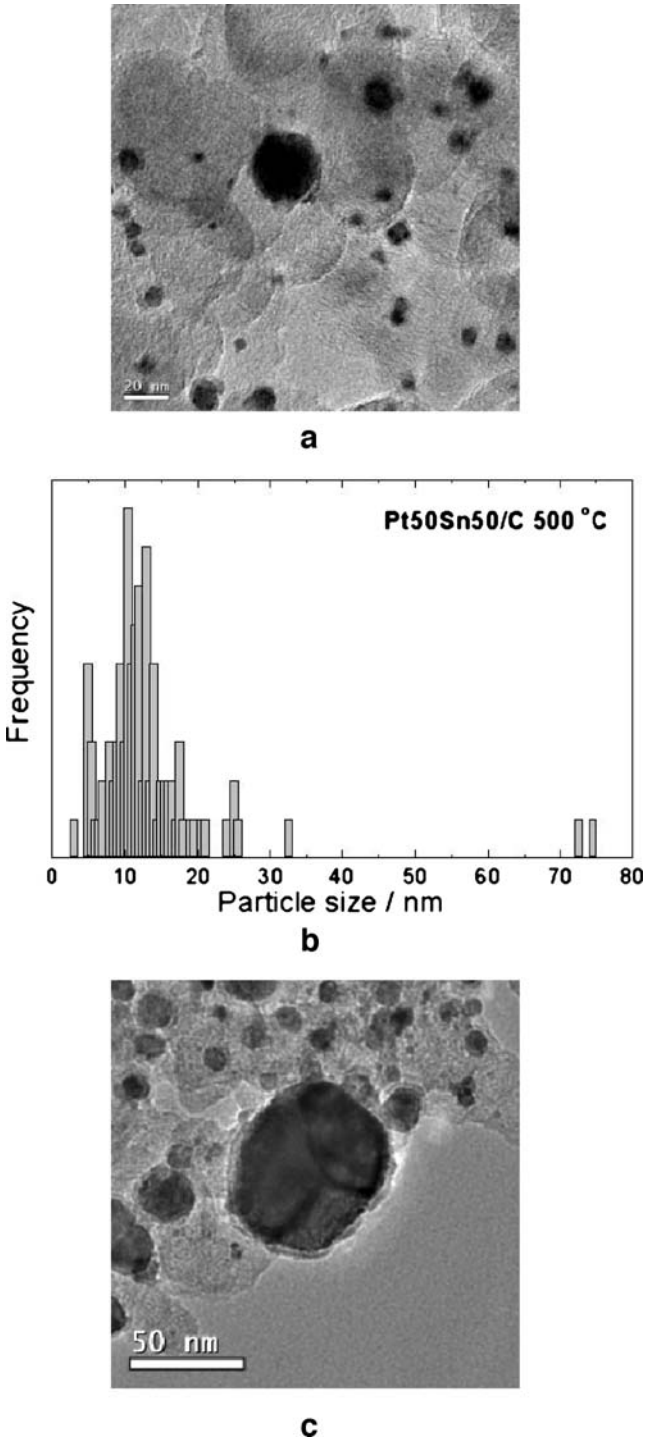

Fig. 4 **a** Low-magnification HRTEM micrograph. **b** Particle size distribution determined from the HRTEM micrographs. *Inset* Particle size distribution for particle size <20 nm. **c** High-magnification HRTEM micrograph of the Pt50Sn505/C catalyst thermally treated at 500 °C

particles (>50 nm) in the Pt–Sn catalyst annealed at 500 °C, faceted on the (111) and (200) planes, characteristic of fcc asymmetric or symmetric cubooctahedral nanocrystals, is shown in Fig. 4c.

Generally, sintering of carbon supported Pt particles takes place at $T>700$ °C [20]. The anomalous growth of some particles could be due to a weak Pt anchorage on the support, related to the preparation method. Indeed, a carbon supported Pt–Co catalyst prepared by the FAM showed a remarkable increase of particle size, from 7.9 to 13.2 nm, after thermal treatment at 500 °C [21]. However, in the present case, the growth of some particles was more significant (from 6.6 to 25–75 nm), so another explanation has to be found. It has to be remarked that at 500 °C in a hydrogen atmosphere metal tin, formed by reduction of SnO_2, is above the normal melting point (231.9 °C) and is present as a liquid phase. It is known in the powder metallurgy of materials that metals are introduced as sintering activators, due to the formation of a liquid phase [22, 23]. Then, it can be inferred that the presence of molten tin promotes the sintering of some Pt–Sn particles. Sintering may occur in a region of the carbon surface where a high number of metal particles and enough liquid tin are simultaneously present. The formation of carbon supported PtSn catalysts having large particle sizes was observed also by Boxall et al. [11]. Their preparation method of PtSn/C catalysts included a thermal treatment at 650 °C. As non-alloyed Sn may be present, it may give rise to sintering of the resulting PtSn particles, which had average domain sizes of 13–27 nm. Neglecting the non-alloyed tin, from the values of the particle sizes obtained by TEM the true surface area of the catalysts was calculated using the equation:

$$\mathrm{SSA}\left(\mathrm{cm}^2\,\mathrm{mg}^{-1}\right) = 610^4/\rho d \qquad (2)$$

where d is the average particle size expressed in nm, and ρ is the density of either the fcc Pt–Sn solid solution (19.2 g cm^{-3}) or those of the $PtSn/Pt_3Sn$ phase mixtures (14.6 and

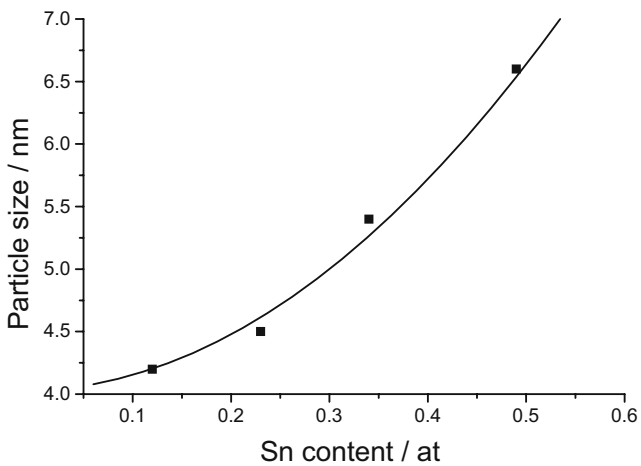

Fig. 5 Dependence of the average Pt–Sn particle sizes (TEM) of the Pt–Sn/C catalysts prepared by the FAM on Sn content in the catalyst (EDX). The values of particle sizes of the Pt–Sn/C catalysts with nominal Pt/Sn>1 were obtained from [14]

14.0 g cm^{-3} for the catalysts thermally treated at 200 and 500 °C, respectively). The obtained values were 473 cm^2 mg^{-1} for the as-prepared catalyst, and 479 and 316 cm^2 mg^{-1} for the catalysts thermally treated at 200 and 500 °C, respectively.

The electrochemical activity for ethanol oxidation of the as-prepared and thermally treated Pt50Sn50/C catalysts was investigated by LSV measurements at room temperature and 40 °C. Figure 6 shows the linear sweep voltammograms for ethanol oxidation at room temperature (Fig. 6a) and 40 °C (Fig. 6b) on as-prepared and thermally treated Pt50Sn50/C prepared by the FAM and Pt75Sn25/C and Pt50Ru50/C from ETEK catalysts. For DEFC application, the working potentials of interest of the anode are located between 0.3 and 0.5 V vs RHE to obtain a cell voltage from 0.6 to 0.4 V assuming a potential of about 0.9–1.0 V vs RHE for the cathode, at the highest current density. In this range of potentials, the activity for the EOR of the as-prepared Pt50Sn50/C catalyst was higher than that of Pt75Sn25/C and Pt50Ru50/C by E-TEK. For potentials up to 0.50–0.55 V, the EOR activity of as-prepared Pt–Sn catalyst was remarkably higher than that of both thermally treated catalysts and that of the Pt–Sn/C catalysts, also prepared by the FAM, with Pt/Sn>1, reported in [14]. As already mentioned, the presence of SnO_2 was detected in the as-prepared catalyst but not in the annealed samples. Moreover, the Pt75Sn25/C catalyst by ETEK is formed almost completely by the Pt_3Sn phase, and the presence of SnO_2 is not detectable [17]. It is known that the presence of oxidized Sn increases the activity of Pt for the EOR. Indeed, Jiang et al. [24] compared the catalytic activity of a partially alloyed PtSn catalyst with that of a quasi non-alloyed $PtSnO_x$ catalyst. The results of chronoamperometry and the performance in direct ethanol fuel cells showed that the $PtSnO_x$ catalyst has a higher catalytic activity for ethanol electrooxidation than the Pt–Sn alloy. They deduced that the unchanged lattice parameter of Pt in the $PtSnO_x$ catalyst is favorable to ethanol adsorption, and meanwhile, tin oxide in the vicinity of Pt nanoparticles could conveniently offer oxygen species to remove the CO-like species of ethanolic residues to free Pt active sites. The pathway of ethanol oxidation should be different on hexagonal PtSn than on cubic Pt_3Sn and on fcc Pt–Sn/SnO_2. It is known that on Pt_3Sn [25] and on Pt–Sn/SnO_2 [26], the main reaction products are acetaldehyde and acetic acid; in the case of the ethanol oxidation on hexagonal PtSn, the reaction mechanism could lead to CO_2 as the main reaction product and to a lower EOR activity, as in the case of ethanol oxidation on Pt–Rh alloys [27, 28]. It has to be remarked, however, that there is no strict relation between the EOR mechanism and the EOR activity. For potentials lower than 0.45 V vs RHE, the EOR activity of the thermally treated catalysts was higher than those of commercial Pt75Sn25/C and Pt50Ru50/C. For E<0.45, the thermally treated catalysts

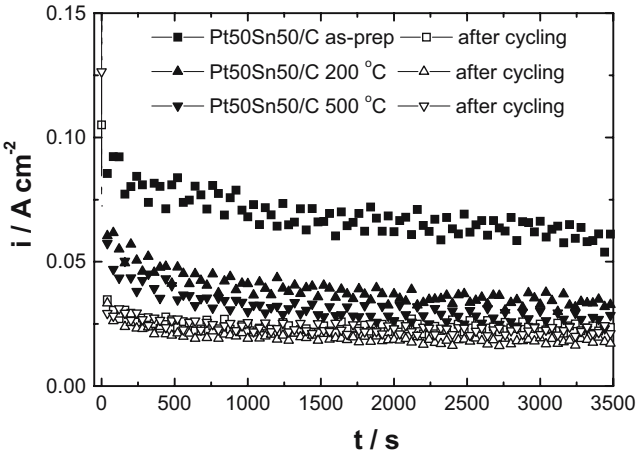

Fig. 7 Chronoamperometry curves for ethanol oxidation on as-prepared and thermally treated Pt50Sn50/C catalysts in 1.0 M ethanol at 90 °C and 0.50 V vs RHE before and after the potential cycling test

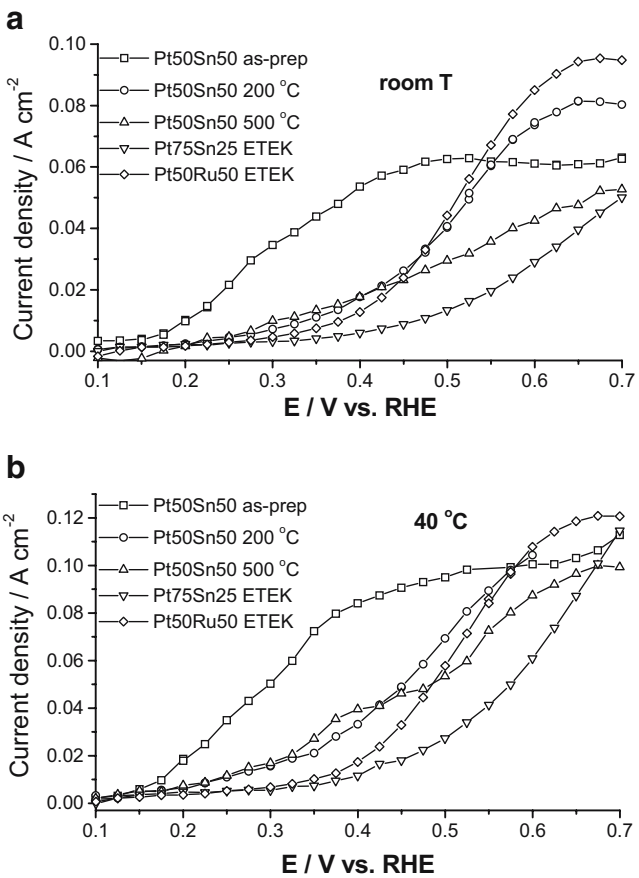

Fig. 6 Linear sweep voltammograms for ethanol oxidation on as-prepared and thermally treated at 200 and 500 °C Pt50Sn50/C catalysts by FAM and commercial Pt–Sn/C (75:25) and Pt–Ru/C (50:50) by E-TEK electrocatalysts in 1.0 M ethanol at **a** room temperature and **b** 40 °C

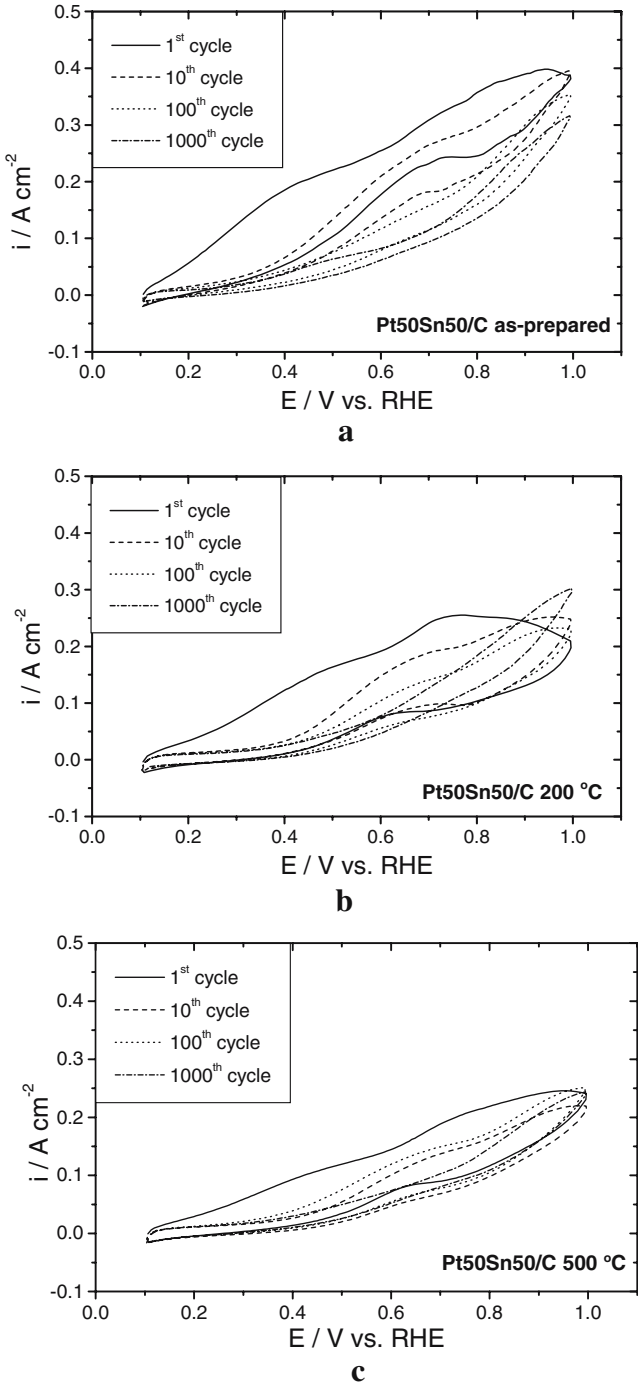

Fig. 8 CV curves (1st, 10th, 100th, and 1,000th cycle) of as-prepared (**a**) and thermally treated at 200 °C (**b**) and 500 °C (**c**) catalysts with a sweep rate of 20 mV s^{-1} at 90 °C

presented almost the same EOR activity, while for E>0.45 V, the EOR activity of the Pt–Sn catalyst annealed at 200 °C was higher than that of Pt–Sn thermally treated at 500 °C, due to the lower active surface area of the latter catalyst.

To compare the potentiostatic behavior of as-prepared and thermally treated Pt50Sn50/C catalysts and to elucidate the potential effect on ethanol oxidation activity on these catalysts, chronoamperometric (CA) experiments for the ethanol oxidation at 90 °C and 0.5 V were carried out and the results are shown in Fig. 7. It can be clearly seen that the currents for ethanol oxidation on all the catalysts dropped rapidly at first and then became relatively stable. The initial surge of the current is possibly due to the charging current or the catalyst poisoning during ethanol oxidation. Consistent with the LSV results, it was found that the current for ethanol oxidation on the as-prepared Pt–Sn/C catalyst is significantly higher than on thermally treated samples.

To investigate the stability of as-prepared and thermally treated Pt50Sn50/C catalysts, these materials were submitted to 1,000 cycles between 0.1 and 1.0 V vs RHE. Figure 8a–c display the first and last CV curves at 90 °C of the as-prepared and thermally treated Pt–Sn/C catalysts. As can be seen in Fig. 8a, the current for ethanol oxidation on the as-prepared Pt–Sn/C catalyst changes considerably after the cycling test. In contrast, there was less performance loss on the thermally treated Pt–Sn/C catalysts, particularly on the catalyst thermally treated at 500 °C. The decrease of EOR activity on the as-prepared catalyst was ascribed to SnO_2 loss on cycling. Indeed, as reported by Wang et al. [29], if Sn is not alloyed with Pt in the catalyst, it is unstable and dissolves in the acid environment of the cell, particularly for potentials higher than 0.5 V. On the other hand, the amount of non-alloyed Sn in the thermally treated samples is considerably lower, and as a consequence, a lower decrease of the EOR activity was observed.

The CA experiments after cycling, also shown in Fig. 7, show that the current for ethanol oxidation is similar for the as-prepared and thermally treated catalysts. This means that the activity of the Pt–Sn solid solution without SnO_2 for the EOR is similar to that of the $PtSn/Pt_3Sn$ phase mixtures.

Conclusions

Formation of fcc Pt–Sn solid solution and SnO_2 was observed in Pt–Sn catalysts prepared by the FAM. Thermal treatment of the carbon supported Pt–Sn alloy catalyst in the atomic ratio Pt/Sn 50:50 gave rise to the formation of cubic (fcc) Pt_3Sn and hexagonal (hcp) PtSn phases. The relative amount of the PtSn phase increased with increasing thermal treatment temperature. To avoid an excessive growth of the metal particles, it is recommended to perform the thermal treatment at temperatures lower than the tin melting temperature. The activity for ethanol oxidation of the as-prepared Pt50Sn50/C catalyst was higher than that of thermally treated catalysts and of commercial Pt75Sn25/C and Pt50Ru50/C catalysts.

Acknowledgments The authors thank the Conselho Nacional de Desenvolvimento Científico e Tecnológico (CNPq, Proc. 142266/2003–5 and Proc. 300477/2005–8), for financial assistance to the project. Thanks are also due to the Brazilian Synchrotron Light Laboratory (LNLS, Campinas, SP, Brazil) for the use of the JEM-3010 ARP HRTEM microscope at the LME.

References

1. Lamy C, Rousseau S, Belgsir EM, Coutanceau C, Léger J-M (2004) Electrochim Acta 49:3901
2. Delime F, Léger J-M, Lamy C (1999) J Appl Electrochem 29:1249
3. Vigier F, Coutanceau C, Perrard A, Belgsir EM, Lamy C (2004) J Appl Electrochem 34:439
4. Srinivasan R, De Angelis RJ, Davis BH (1987) J Catal 106:449
5. Srinivasan R, Davis BH (1992) Appl Catal A 87:45
6. Srinivasan R, Sharma R, Su S, Davis BH (1994) Catal Today 21:83
7. Llorca J, de la Piscina PR, Fierro JLG, Sales J, Homs N (1995) J Catal 156:139
8. Borgna A, Stagg SM, Resasco DE (1998) J Phys Chem B 102:5077
9. Llorca J, Homs N, León J, Sales J, Fierro JLG, de la Piscina PR (1999) Appl Catal A 189:77
10. Radmilovic V, Richardson TJ, Chen SJ, Ross Jr PN (2005) J Catal 232:199
11. Boxall DL, Kenik EA, Lukehart CM (2002) Chem Mater 14:1715
12. Zhou W, Zhou Z, Song S, Li W, Sun G, Tsiakaras P, Xin Q (2003) Appl Catal B 46:273
13. Boennemann H, Brinkmann R, Britz P, Endruschat U, Mortel R, Paulus UA, Feldmeyer GJ, Schmidt TJ, Gasteiger HÁ, Behm RJ (2000) J New Mater Electrochem Syst 3:199
14. Colmati F, Antolini E, Gonzalez ER (2007) J Electrochem Soc 145:B39
15. Gonzalez ER, Ticianelli EA, Pinheiro AIN, J. Perez J (1997) Brazilian Patent, P.I. 9.702.816–9
16. Salgado JRC, Gonzalez ER (2003) Ecl Quím 28:77
17. Colmati F, Antolini E, Gonzalez ER (2006) J Power Sources 157:98
18. Kuznetsov VI, Belyi AS, Yurchenko EN, Smolikov MD, Protasova MT, Zatolokina EV, Duplayakin VK (1986) J Catal 99:159
19. Harris IR, Norman M, Brayant AW (1968) J Less-Common Met 16:427
20. Antolini E (2003) Mater Chem Phys 78:563
21. Salgado JRC, Antolini E, Gonzalez ER (2005) J Power Sources 141:13
22. Selecká M, Salak A, Danninger H (2003) J Mater Proc Tech 141:379
23. Campos M, Sanchez D, Torralba JM (2003) J Mater Proc Tech 143-144:464
24. Jiang L, Sun G, Sun S, Liu J, Tang S, Li H, Zhou B, Xin Q (2005) Electrochim Acta 50:5384
25. Alcala R, Shabaker JW, Huber GW, Sanchez-Castillo MA, Dumesic JA (2005) J Phys Chem B 109:2074
26. Rousseau S, Coutanceau C, Lamy C, Leger J-M (2006) J Power Sources 158:18
27. de Souza JPI, Queiroz SL, Bergamaski K, Gonzalez ER, Nart FC (2002) J Phys Chem B 106:9825
28. Colmati F, Antolini E, Gonzalez ER (2007) J All Comp (in press)
29. Wang K, Gasteiger KA, Markovic NM, Ross PN (1996) Electrochim Acta 41:2587